

Numerical Simulation of the Fatigue Life of Corroded Steel Plates

Hua Zhang^{1,2}

¹School of Civil Engineering, Xi'an University of Architecture and Technology, Xi'an, China

²China Coal Xi'an Design Engineering Co., LTD, Xi'an, China

Abstract:

Ten pairs of corroded steel plate specimens were obtained through an artificial accelerated corrosion procedure, and their 3D surface morphologies were measured by a noncontact profiler. A method for reconstructing a geometric model of the corroded surface was proposed and employed to conduct tensile simulations. Fatigue life prediction of the corroded steel plates was realized based on the nominal stress method. The results show that the stress concentration near pits led to a significant decrease in the fatigue life of the steel plates. In the early stage of corrosion, acicular pits were densely distributed on the surface of the steel plate, but in the later stage of corrosion, the fusion of the corrosion pits caused the radius to increase. Consequently, the fatigue life of corroded steel also showed a trend of first declining and then increasing with the corrosion time. The error between the predicted fatigue life of the corroded steel plate and the experimental results was within 15%, which verifies the validity of the proposed method.

Keywords: *Corroded steel, Surface morphology, Fatigue life, Numerical analysis, 3D profile*

I. INTRODUCTION

As service life increases, most steel structures corrode, and under normal use conditions, they may endure high-cycle fatigue that is lower than the yield strength. Compared with a static load, the stress concentration caused by the surface gap of the corroded steel structure will greatly reduce its fatigue performance, posing a serious threat to the safe service of the existing steel structure.

The most direct and reliable way to obtain the fatigue life of corroded steel is through a standard fatigue test. Garbatov et al. corroded steel box girders under real seawater conditions and cut small corroded steel samples from steel box girders with welded stiffeners to conduct fatigue strength studies, proving that there is a direct relationship between the initial corroded surface roughness and the rust pit depth and fatigue life [1]. Beretta et al. conducted fatigue test research on corroded steel wire, and the results showed that the stress concentration is larger for sharper pit shapes, indicating that this is the major cause of the decrease in fatigue strength. However, high-cycle fatigue tests are cumbersome and costly, and corrosion is extremely random [2]. Even different specimens with the same corrosion time can have huge differences in corrosion morphology and fatigue life. If the test sample is small, it is difficult to study the regularity of the fatigue life of the corroded steel plate.

Researchers have also carried out extensive research work in fatigue theory and have proposed a series of theoretical methods, such as the nominal stress method [3-5], the local stress-strain method [6-8], the stress field strength method [8-11], and the virtual crack closure method [13-15]. When applying these methods, the location of the fatigue source or the state of stress and strain must be obtained in advance. The corroded surface is usually very complicated, and it is not easy to directly obtain these indicators.

With the development of computer technology, fatigue life analysis based on the finite element method has gradually developed. The extreme irregularity of the corroded surface requires the finite element mesh to accurately reflect the detailed characteristics of the corroded surface, so the traditional finite element modelling method is not well applicable. To solve the above problems, this paper proposes a geometric reconstruction method of corroded surfaces, combined with the finite element method and fatigue theory, and proposes a numerical prediction method for the fatigue life of corroded steel.

10 groups of corroded steel plate specimens were obtained by the neutral salt spray accelerated corrosion test, and the surface topographies of the corroded steel plates were collected by a 3D noncontact scanner. Then, the point cloud data of the corroded surfaces were processed by reverse engineering software, and the geometric model of the corroded surface was reconstructed. Finally, the corroded surface model was imported into the finite element software to establish a three-dimensional solid model of the corroded steel plate. Through tensile simulation and fatigue analysis, the fatigue life of the corroded steel plate was calculated.

II. EXPERIMENTAL PROCEDURE

2.1 Accelerated Corrosion

In this paper, the neutral salt spray test method (NSS) was used to conduct accelerated corrosion on 11 groups of Q235 steel plates for periods of 0, 14, 28, 42, 56, 70, 84, 98, 118, 138, and 178 days in a simulated marine atmosphere. The size (T×L×W) of the plates was 8 mm×280 mm×50 mm. There were 2 specimens for each age, and the specimen number is A_{ij} , where i represents the corrosion age, $i=0,1,2... 10$, and j represents the number of the specimens in each group, $j=1,2$. To measure the corrosion depth, epoxy resin was used to wrap a 1cm area on the edge of specimen A_{i1} as the corrosion area reference level. The mass loss rate of the other specimen was measured. The temperature in the salt spray test box was kept at 35 ± 1 °C, and the relative humidity was approximately 95%. The spray was a 5% NaCl solution with pH 7.0 ± 0.2 . The specimens were placed on an insulating support at an angle of 30, as shown in Fig 1. During the test, the steel plate was turned over once a day to ensure that the corrosion conditions were the same on both sides.



Fig 1: Placement of test pieces in the salt spray box

2.2 3D surface Profile Measurements

The PS50 3D noncontact surface topography instrument (Fig 2) made by NANOVEA was used to scan the surface topography of the corroded steel plate Ai1. Considering that the maximum measurement area of the instrument is 40 mm and 30 mm (width and length), to measure the corrosion characteristics of the whole corroded specimen, two areas containing datum planes were selected with one area coming from each side of the specimen. The measurement area is shown in Fig 4, and the test step is 18. Based on the output XY coordinate data, the corrosion depth of each test point was obtained, and the 3D topography of the corroded surface was drawn.



Fig 2: PS50 profiler for surface measurement

2.3 Fatigue Test

According to the standard GB/T3075-2008 ("Axial Force Control Method for Fatigue Test of Metal Materials"), a hydraulic servo universal fatigue testing machine (HT-977), as shown in Fig 3, was used to conduct fatigue tests on the Ai1 specimen. The load form was a sinusoidal wave, the stress ratio was $R=0.1$, the maximum stress level was 260 MPa (0.6 times the ultimate strength), and the loading frequency was 10

Hz. The size of the fatigue specimen is shown in Fig 4. When machining, the fatigue specimen was a parallel section to ensure that the corrosion datum was not included.



Fig 3: Fatigue test setup

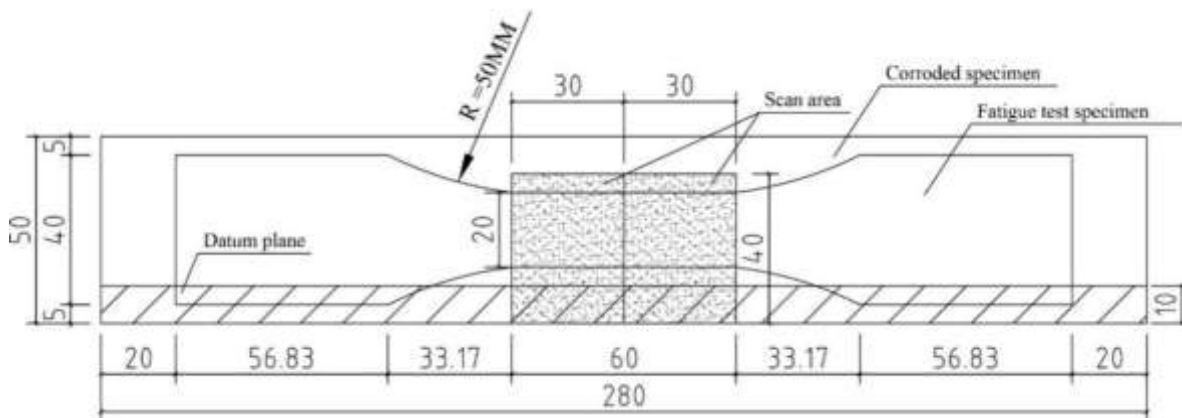


Fig 4: Surface measurement region of the corroded samples and dimensions of the fatigue test specimens (unit: mm)

III. EXPERIMENTAL RESULTS AND DISCUSSION

3.1 Corrosion Morphology

The mass loss rate is used to characterize the corrosion degree of the steel plate:

$$\eta = \frac{m_0 - m_1}{m_0} \times 100\% \quad (1)$$

Where m_0 is the mass of the specimen before corrosion; m_1 is the mass of the specimen after corrosion; and η is the mass loss rate. Fig 5 shows the relationship between the mass loss rate of the specimen and the corrosion time. The mass loss rate and the corrosion time show a rough power law functional relationship.

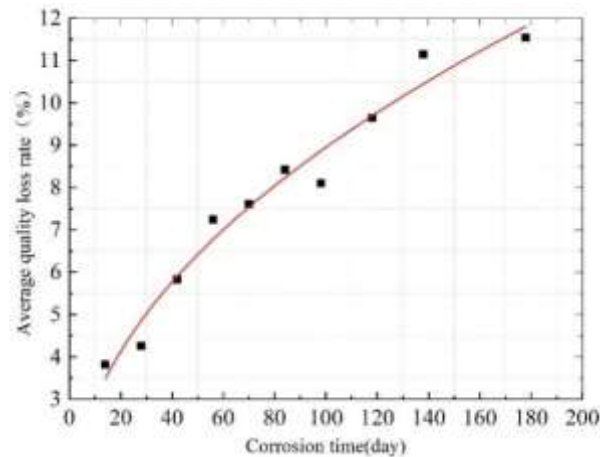
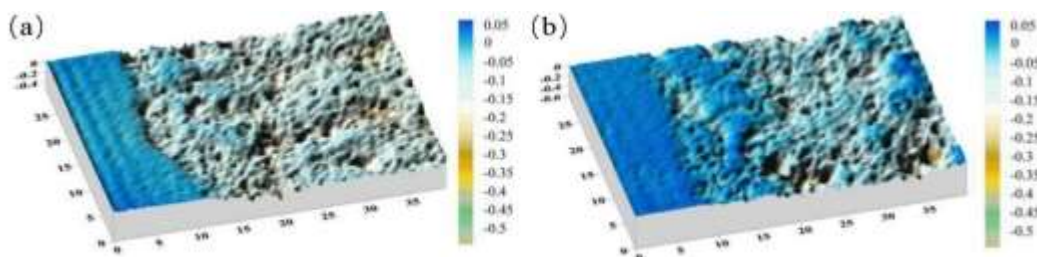


Fig 5: Relationship between the mass loss rate and corrosion time

Fig 6 shows surface morphology of the corroded specimens. The three-dimensional topography was composed of two parts, namely, the reference plane wrapped with epoxy resin and the corroded area. From specimens A11 to A101, the colour of the corroded area gradually deepened, indicating that the corrosion depth continued to deepen. In the early stage of corrosion, dense pinhole-like corrosion pits were seen on the surface, but as the corrosion age increased, the lateral growth of the corrosion pits led to their fusion, so the radius of the corrosion pits gradually increased.



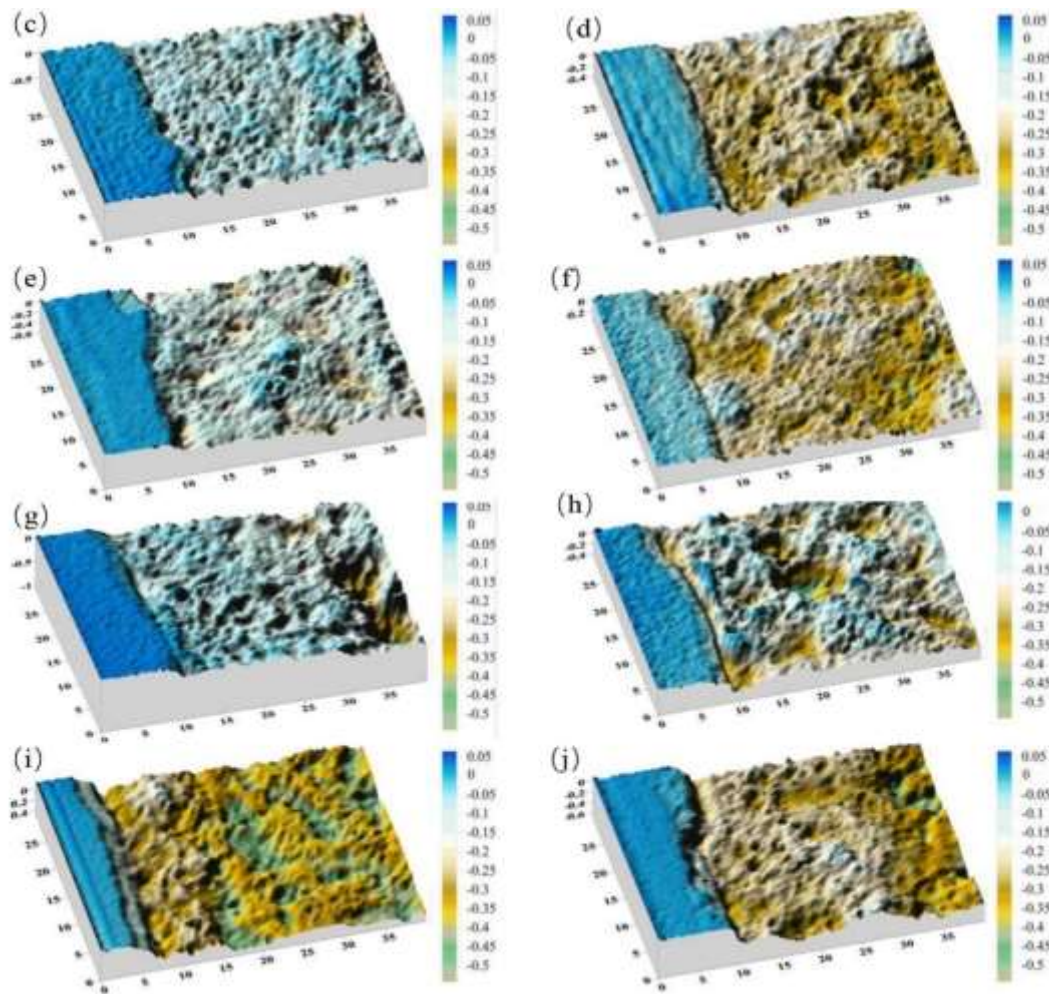


Fig 6: Surface morphology of the corroded specimens: (a) A11, (b) A21, (c) A31, (d) A41, (e) A51, (f) A61, (g) A71, (h) A81, (I) A91, (j) A101

3.2 Fatigue Performance of the Corroded Steel

The fatigue test results are shown in Table I. The fatigue life of the corroded steel plates was greatly reduced. Their fatigue life was only approximately 3.5% to 21% compared with control specimens. With the extension of the corrosion time, the fatigue life shows a trend of first decreasing and then increasing. This is because the corrosion pits are sharper at the initial stage of corrosion, and the stress concentration phenomenon is more obvious and has a significant impact on the fatigue life. In the later stage of corrosion, the corrosion pits merged horizontally, the overall corrosion phenomenon was more obvious, the stress distribution was more uniform, and the fatigue life also increased. Therefore, in actual engineering inspection, the effect of early corrosion on fatigue performance cannot be ignored because there is only a small amount of early corrosion.

Table I. Results of fatigue test

Corrosion time/d	Specimen No.	Fatigue life/cycles
0	A01	6730000
14	A11	291200
28	A21	356000
42	A31	416550
56	A41	340500
70	A51	426100
84	A61	738400
98	A71	240230
118	A81	705450
138	A91	1449300
178	A101	571000

IV. NUMERICAL SIMULATION OF THE FATIGUE LIFE OF THE CORRODED STEEL PLATES

4.1 Reconstruction of the Corroded Surface

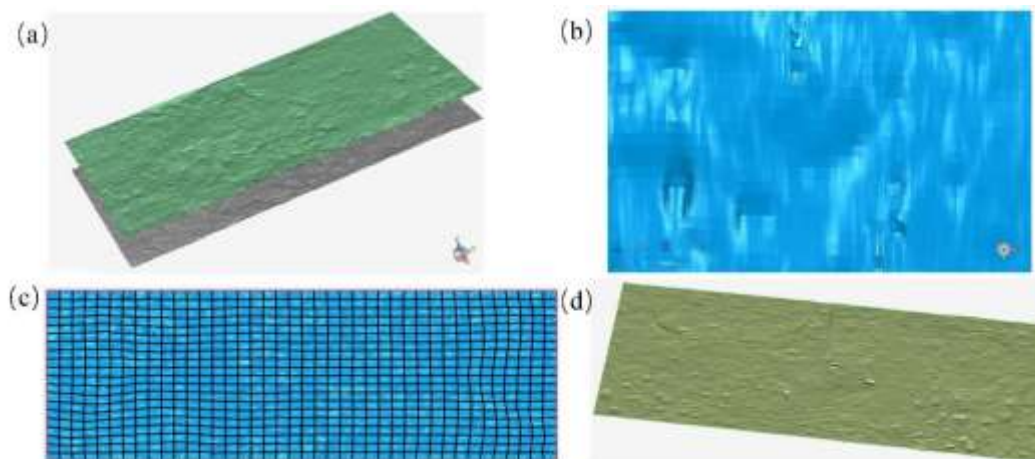


Fig 7: The basic process of the NURBS surface reconstruction of the Corrosion test piece surface: (a) Removing the datum surface data, (b) Partial detailed view of the triangle stage, (c) Layout of regular surface patches, (d) NURBS surface of the rusted surface

Geomagic Studio software was used to postprocess the measured high-precision three-dimensional point cloud data on the surface of the corroded steel plate and to reconstruct the corrosion morphology features [16].

(1) Similar to the fatigue test specimens, the datum surface data should be eliminated first, only the corrosion morphology data from the parallel section should be kept, and the data from two measurements on each surface should be spliced.

(2) During the measurement process, there will always be more or less incorrect points, which will interfere with the final surface simulation. Therefore, it is necessary to filter out isolated noise points by setting a threshold.

(3) The packaged surface is usually broken, and gap are filled by the "fill hole" command. Then, the smoothness of the surface is improved by subdividing the triangle.

(4) Finally, a precise surface layout is constructed, contour lines and curvature lines are detected, surface patches are constructed, data segmentation and surface reconstruction are realized, and neat meshing is obtained by constructing grids, thereby fitting a smooth NURBS surface.

Fig 7 shows the reconstruction process of the NURBS curved surface of the corroded 42-day specimen. To verify the accuracy of the geometric model, the reconstructed rusted surface model and the original point coordinates were imported into Geomagic Qualify for error detection. Fig 8 shows the error of random grabbing points on the corrosion surface of specimen A31 as an example. The errors in the Dx and Dy directions are negligible compared with the Dz direction, and the total error of the points is determined by the Dz direction. Fig 9 shows the frequency distribution of points in different error regions. The errors are concentrated between -0.05 mm and 0.05 mm. The measurement points account for more than 93%, and the points with an error within ± 0.004 mm account for approximately 25%, indicating that the reconstruction accuracy is very high.

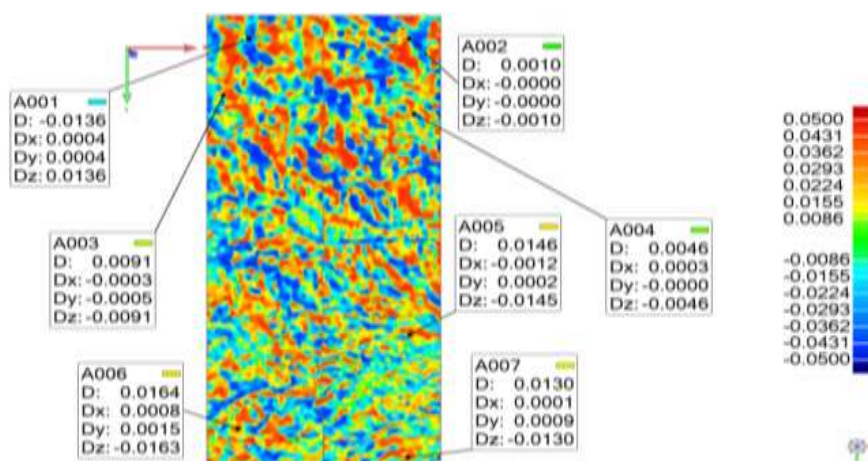


Fig 8: Error of randomly grabbed points

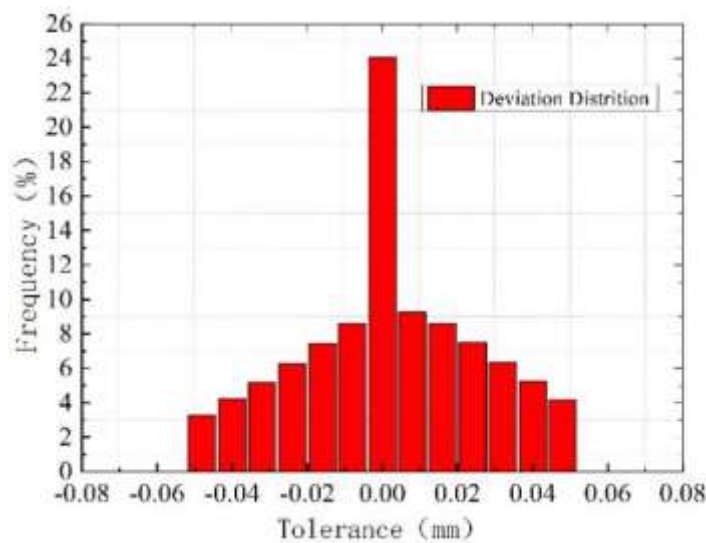


Fig 9: Frequency distribution in different error regions

4.2. Stress Concentration Simulation

4.2.1 Establishment of finite element model

The surface model files (60 mm×20 mm) for the upper and lower surfaces of each specimen were imported into ANSYS. The distance between the two surfaces was determined by the uncorroded reference surface, and three-dimensional modelling was realized by Boolean operation. A geometric model of a corrosion specimen is shown in Fig 10(a). A 20-node SOLID95 solid element was used to establish the corroded steel plate model, and a tetrahedral mesh was used to freely divide the geometric model. To improve the accuracy and reduce the computational cost, the mesh length of the corroded surface was 0.2 times the area away from the corroded surface, as shown in Fig 10(b), and the number of division units for each model was approximately 160,000. A solid end constraint was applied to one end of the model ($y=0$), and a uniform stress was applied to the other end ($y=60$ mm). The constitutive model adopts the measured stress-strain curve of the steel tensile test, as shown in Fig 11.

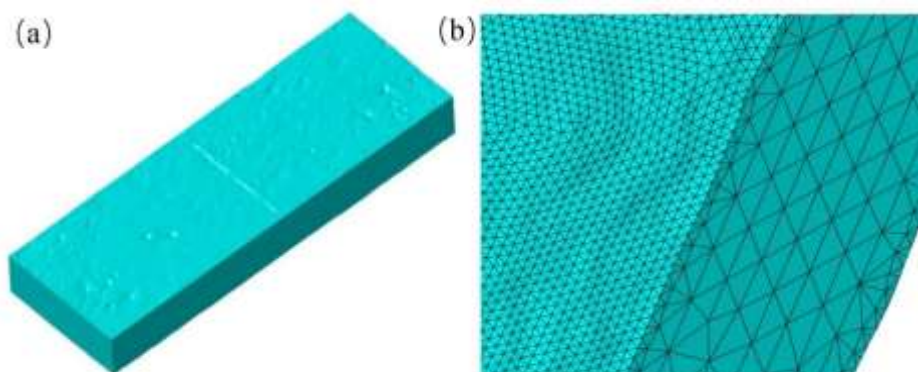


Fig 10: Geometric model of corroded steel plate (a) and refined meshing (b)

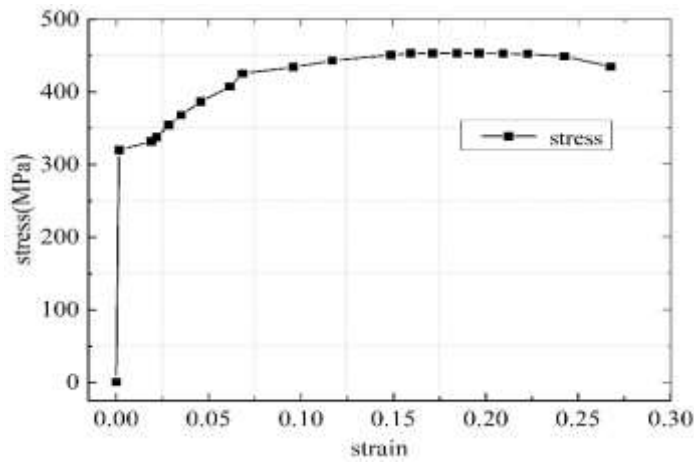
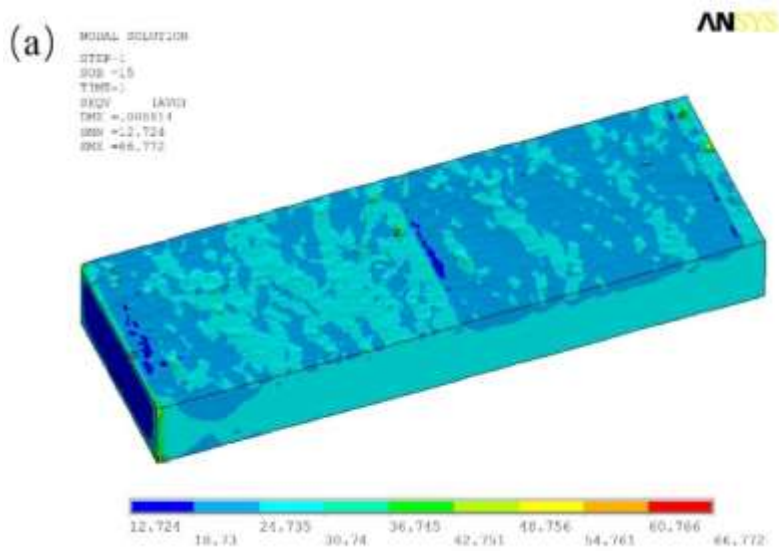


Fig 11: Stress-strain curve of the steel

4.2.2 Calculation results



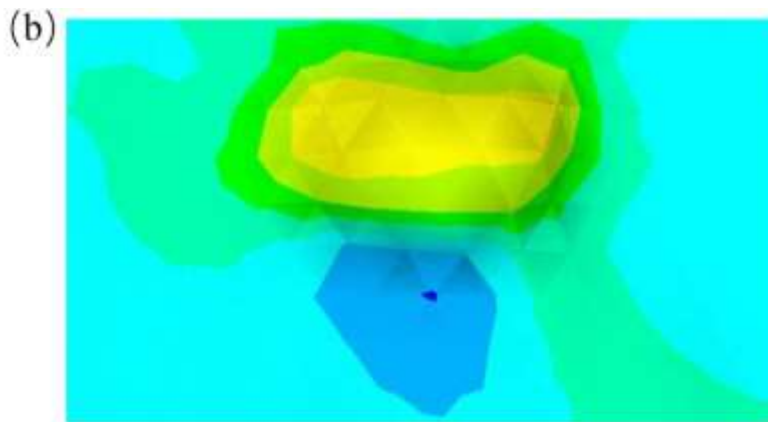


Fig 12: Stress cloud diagram (a) and model stress concentration in a local pitting area (b) when the uniform stress was 26 MPa

A tensile force of 26 MPa was applied to the geometric models of the 10 corroded specimens to perform static calculations. Fig 12(a) shows the surface stress cloud diagram using specimen A41 as an example. Points with greater stress concentrations were concentrated on the corroded surface, and local magnification revealed obvious stress concentrations near the corrosion pits, as shown in Fig 12(b). The maximum stress point of the corrosion pits was selected to calculate the stress concentration factor of the corroded surface, and the results are shown in Table II.

Table II. Stress concentration factor

Specimen	Time (d)	Stress concentration factor Kt
A11	14	2.12
A21	28	2.03
A31	42	1.74
A41	56	1.69
A51	70	1.41
A61	84	1.15
A71	108	1.45
A81	128	1.44
A91	148	1.43
A101	178	1.43

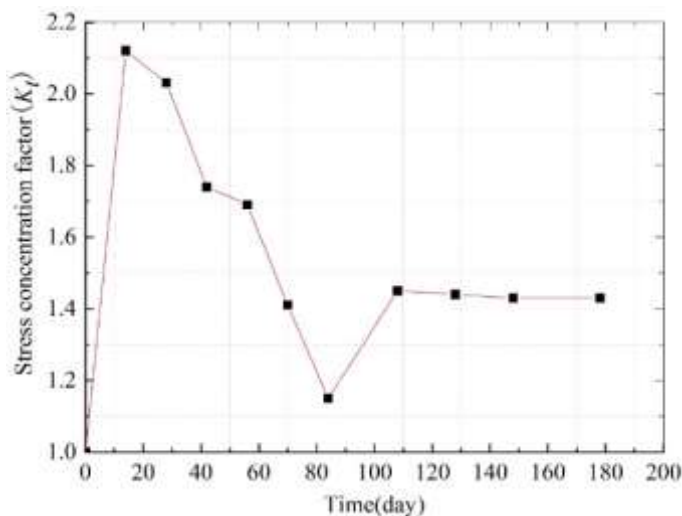


Fig 13: Variation curve of the stress concentration factor with the corrosion time

Fig 13 shows the change law of the stress concentration factor with the corrosion time. At 14 days of corrosion, the stress concentration factor reached the maximum value of 2.12, and then the stress concentration factor value gradually decreased to 1.15, which is approximately the same trend seen in the changes of the fatigue life of the corroded steel. This shows that the steel gradually changed from initial pitting to full-scale corrosion.

Subsequent application of a 260-MPa uniform stress to the model showed that multiple corrosion pits have become plastic, as shown in Fig 14. The stress at the determined node number was extracted and saved to complete the static analysis.

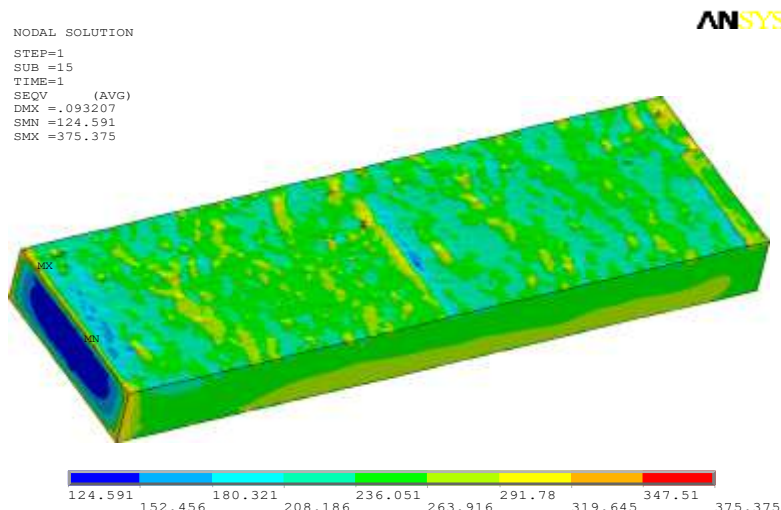


Fig 14: Stress cloud diagram when the uniform stress was 260 MPa

4.3 Fatigue Life Prediction

The S-N curve is the basic data for fatigue life prediction [17]. Generally, the S-N curve of steel is measured by a standard test method, that is, a uniaxial tension-compression test with a stress ratio $R=-1$. Reference conducted a fatigue performance test on Q235 low carbon steel and gave the fatigue life of steel under different stress amplitudes σ_a [18]. The basic S-N curve of Q235 steel when $R=-1$ can be obtained by fitting the data, as shown in Fig 15.

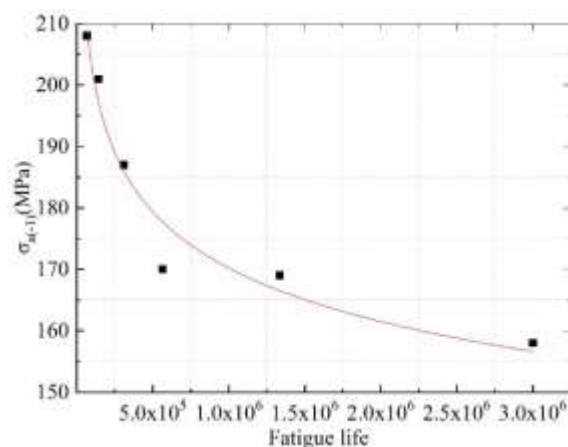


Fig 15: S-N curve of Q235 steel when $R=-1$

$$\lg N = 36.25085 - 13.16678 \lg S \tag{2}$$

In this paper, the Goodman straight line model was used to correct the average stress and to convert the average stress under the condition $R=0.1$. According to the Goodman straight line model, the stress amplitude under different stress ratio conditions satisfies the following relationship:

$$\frac{\sigma_a}{\sigma_{a(-1)}} + \frac{\sigma_m}{\sigma_u} = 1 \tag{3}$$

Where $\sigma_{a(-1)}$ is the stress amplitude corresponding to $R=-1$, σ_u is the ultimate strength of Q235 steel, and σ_m is the average stress corresponding to $R=-1$. Substituting Formula (3) into Formula (2), the S-N curve corresponding to the stress ratio of steel at $R=0.1$ is obtained:

$$\lg N = 36.25085 - 13.16678 \lg \frac{\sigma_a}{1 - 0.0027161 \sigma_a} \tag{4}$$

The ANSYS Fatigue module was used to predict the fatigue life of corroded steel [19]. This model uses

the nominal stress method to predict the fatigue life. The S-N curve corresponding to Q235 steel with R=0.1 was imported into the Fatigue module in the form of a list. According to the fatigue position parameters determined by the static analysis, the node corresponding to the maximum stress concentration factor of the corroded surface was selected as the fatigue analysis object, and the fatigue life was finally determined.

4.4 Comparison between Finite Element Simulation and Experimental Results

Table III compares the fatigue life simulation results and test results of corroded steel. The finite element simulation values are all greater than the experimental values, but the errors are all within 15%. The numerical prediction method for the fatigue life of corroded steel proposed in this paper is determined to be feasible.

Table III. Comparison of the predicted numerical results and test results of the fatigue life of corroded steel

Model number	Numerical fatigue life prediction	Test fatigue life value/life/cycles
A11	321400	291200
A21	376700	356000
A31	467800	416550
A41	379400	340500
A51	465100	426100
A61	783300	738400
A71	258400	240230
A81	756400	705450
A91	1634000	1449300
A101	636600	571000
A11	321400	291200

V. CONCLUSION

1) A three-dimensional noncontact scanner was used to collect the surface morphology of corroded steel plates. In the early stage of corrosion, needle-shaped rust pits were densely distributed on the surface of the steel plate, but in the later stage of corrosion, the fusion of these rust pits caused the radius to increase.

2) The fatigue life of the steel plate after corrosion was greatly reduced, and with an extension of corrosion time, the fatigue life showed a trend of first decreasing and then increasing, which is basically consistent with the evolution of the surface corrosion characteristics.

3) A reconstruction method using a geometric model of the corroded surface is proposed, its accuracy was verified, and a numerical simulation of the tensile strength of the corroded steel plate was realized. The results show that the stress concentration phenomenon was most obvious near the rust pits.

4) The fatigue life of the corroded steel plate was predicted based on the stress distribution on the surface of the corroded steel plate. The results show that the predicted value was basically consistent with the experimental value, which verifies the effectiveness of the proposed method.

REFERENCES

- [1] Garbatov, Y., Soares, C. G., Parunov, J. (2014) Fatigue strength experiments of corroded small scale steel specimens. *International Journal of Fatigue* 59: 137-144.
- [2] Beretta, S., Carboni, M., Fiore, G., Conte, A. L. (2010) Corrosion-fatigue of A1N railway axle steel exposed to rainwater. *International Journal of fatigue* 32(6): 952-961.
- [3] Ke, C., Feng, W. (2010) Structure Finite Life Design—Nominal Stress Method. *China Heavy Equipment*, 2 [in Chinese].
- [4] Bagherifard, S., Guagliano, M. (2014) Application of different fatigue strength criteria on shot peened notched parts. Part 2: nominal and local stress approaches. *Applied surface science* 289: 173-179.
- [5] Tian, B. J., Xiong, J. J., Liu, J. Z. (2015) A new approach for evaluating fatigue lives of multi-fastener mechanical joints based on a nominal stress concept and minimal datasets. *International Journal of Fatigue* 80: 257-265.
- [6] Zheng, M., Li, P., Yang, J., Li, H., Qiu, Y., Zhang, Z. (2017) Fatigue life prediction of high modulus asphalt concrete based on the local stress-strain method. *Applied Sciences* 7(3): 305.
- [7] Schneider, R., Wuttke, U., Berger, C. (2010) Fatigue analysis of threaded connections using the local strain approach. *Procedia Engineering* 2(1): 2357-2366.
- [8] Socie, D. F. (1977) Fatigue-life prediction using local stress-strain concepts. *Experimental Mechanics* 17(2): 50-56.
- [9] Zeng, Y., Li, M., Zhou, Y., Li, N. (2019) Development of a new method for estimating the fatigue life of notched specimens based on stress field intensity. *Theoretical and Applied Fracture Mechanics* 104, 102339.
- [10] Zhao, D., Liu, S., Xu, Q., Shi, F., Sun, W., Chai, L. (2017) Fatigue life prediction of wire rope based on stress field intensity method. *Engineering Failure Analysis* 81: 1-9.
- [11] Shen, W., Barltrop, N., Yan, R., Liu, E., Qin, K., Song, L. (2015) Stress field and fatigue strength analysis of 135-degree sharp corners based on notch stress strength theory. *Ocean Engineering* 107: 32-44.
- [12] Shang, D. G., Wang, D. K., Li, M., Yao, W. X. (2001) Local stress-strain field intensity approach to fatigue life prediction under random cyclic loading. *International Journal of Fatigue* 23(10): 903-910.
- [13] Krueger, R. (2004) Virtual crack closure technique: History, approach, and applications. *Appl. Mech. Rev* 57(2): 109-143.
- [14] Krscanski, S., Brnic, J. (2020) Prediction of Fatigue Crack Growth in Metallic Specimens under Constant Amplitude Loading Using Virtual Crack Closure and Forman Model. *Metals* 10(7), 977.
- [15] Qian, Q., Xie, D. (2007) Analysis of mixed-mode dynamic crack propagation by interface element based on virtual crack closure technique. *Engineering Fracture Mechanics* 74(5): 807-814.
- [16] Sousa, M. V. S., Vasconcelos, E. C., Janson, G., Garib, D., Pinzan, A. (2012) Accuracy and reproducibility of 3-dimensional digital model measurements. *American Journal of Orthodontics and Dentofacial Orthopedics* 142(2): 269-273.
- [17] Murakami, Y., Takagi, T., Wada, K., Matsunaga, H. (2021) Essential structure of SN curve: Prediction of fatigue life and fatigue limit of defective materials and nature of scatter. *International Journal of Fatigue* 146, 106138.
- [18] Wang B. L. (2008) Experimental study on the influence of corrosion on the fatigue life and crack growth rate of low carbon steel. MA thesis. Shandong University, Shandong, China [in Chinese]
- [19] Ye, X. Y., Zhang, J. H., Jiang, X. P., Ding, Y. N. (2011) Calculation of Crankshaft Fatigue Life Based on ANSYS-FATIGUE. *Fluid Machinery*, 4.